

Collocation and Mass Matrix in Least-squares Isogeometric Analysis

Gengchen Li^a, Hongwei Lin^{a,*}

^a*School of Mathematical Sciences, Zhejiang University, Hangzhou, 310058, China*

Abstract

In this paper, we conduct a systematic numerical analysis of the spectral properties of the collocation and mass matrices in the isogeometric least-squares collocation method (IGA-L), for the approximation of the Poisson problem with homogeneous Dirichlet boundary conditions. This study primarily focuses on the spectral properties of the IGA-L collocation and mass matrices in relation to the isogeometric discretization parameters, such as the mesh size, degree, regularity, spatial dimension, and the number and distribution of the collocation points. Through a comprehensive numerical investigation, we provide estimations for the condition number, as well as the maximum and minimum singular values, in relation to the mesh size, degree and regularity. Moreover, in this paper we also study the effect of the number and distribution of the collocation points on the spectral properties of the collocation matrix, providing insights into the optimization of the collocation points for achieving better-conditioned linear systems.

Keywords: Isogeometric analysis, Isogeometric least-squares collocation method, Condition number, Spectral properties

1. Introduction

Isogeometric analysis (IGA), introduced in [1], is an emerging numerical technique providing connection between computer-aided design (CAD) and computer-aided engineering (CAE). The main idea of IGA is to directly handle the CAD geometry represented by non-uniform rational B-splines (NURBS), and apply the same basis functions for numerical simulation, thereby achieving seamless integration of CAD and CAE. Since Hughes et al. introduced IGA [1], extensive studies have shown its advantages in many problems and applications [2, 3, 4]. Compared to finite element method, IGA offers not only the standard h - and p -refinement, but also k -refinement, which enables smoother basis functions and higher accuracy [5].

Recent studies have explored the isogeometric analysis collocation method (IGA-C) to address the challenge of obtaining sparser stiffness matrices compared to those arising from traditional IGA Galerkin methods [6, 7, 8, 9]. IGA-C involves substituting collocation points into the strong form of a partial differential equation (PDE), which results in a simple and flexible formulation of the collocation matrix. Moreover, since the collocation matrix requires only one function evaluation per collocation point, the computational cost of IGA-C is relatively low. The number of collocation points can be set equal to or greater than the degrees of freedom (dof), with the latter referred to as the isogeometric least-squares collocation method (IGA-L) [9, 10].

For collocation methods, the distribution of the collocation points plays a crucial role in improving the stability and convergence rate. An appropriate distribution of these points can enhance the numerical performance significantly. Popular options, such as Greville abscissae and Demko [6, 11], super-convergent (SC) points [9], Cauchy-Galerkin (CG) points [12] have been widely utilized and provided significant improvements since their introduction.

Since the introduction of the IGA, most of the studies have primarily focused on its applications [2, 3, 4, 13, 14], with rel-

atively little attention given to the theoretical estimation of the spectral properties of the IGA matrices, such as the condition number. However, the accuracy and computational cost of solving the linear system arising from the isogeometric discretization are crucial, especially for large-scale problems, with the condition number playing a key role in both. For direct solvers, an increase in the condition number leads to a decrease in the number of significant digits in the solution, resulting in a less accurate solution [15]. As the degree p increases, the discretization matrix A becomes denser, which increases the computational cost of direct solvers, making them prohibitively expensive, particularly for large problems [15]. Consequently, iterative methods are typically employed for practical solutions. For an iterative solver, the number of iterations required to reach a specified error threshold is also influenced by the condition number. Systems with large condition numbers tend to require more iterations to converge to the desired accuracy [15]. Since the convergence rate of the iterative method is strongly dependent on the condition number, which ultimately impacts the accuracy of the numerical method, it becomes essential to thoroughly investigate the relationship between the condition number and the parameters of the IGA discretized model.

In this study, we aim to systematically investigate the spectral properties of the collocation and mass matrix in IGA-L for Poisson problem with homogeneous Dirichlet boundary conditions in one-, two-, and three-dimensional domains. Specifically, we analyze their behavior with respect to key parameters such as the mesh size h , degree p , spatial dimension d , the number and the distribution of collocation points.

The rest of the paper is organized as follows. Section 1.1 presents related studies. In Section 2 we briefly review the fundamentals of B-splines and NURBS, and introduce the eigenvalue and condition number estimations for the IGA-Galerkin (IGA-G) approximation of the Poisson problem. Section 3 introduces the Poisson equation with Dirichlet boundary conditions and its isogeometric discretization. In Section 4, we analyze the behavior of the singular values and condition numbers of the collocation and mass matrix, providing estimations regarding their dependence on mesh size, degree and regularity.

*Corresponding author.

Email addresses: gengchenli@zju.edu.cn (Gengchen Li), hwlin@zju.edu.cn (Hongwei Lin)

1.1. Related work

Despite the growing applications of IGA, relatively few studies have explored the theoretical properties of the IGA discretization matrix. Gahalaut and Tomar derived bounds for the external eigenvalues and the spectral condition number of the mass and stiffness matrix in the isogeometric discretization of the Poisson problem [16], i.e.,

$$\begin{aligned}\mathcal{K}(\mathbf{M}) &\leq cp^2 16^p \\ \mathcal{K}(\mathbf{K}) &\leq cp^8 16^p,\end{aligned}\quad (1)$$

where c is independent of h and p , and $\mathcal{K}(\mathbf{M})$, $\mathcal{K}(\mathbf{K})$ denote the condition numbers of the mass matrix \mathbf{M} , and stiffness matrix \mathbf{K} , respectively. Garoni et al. studied the spectral properties of the stiffness matrix for classical second-order elliptic problems [17]. They employed the concept of a symbol in the Toeplitz setting to examine the non-singularity, conditioning and spectral distribution in the Weyl sense. Eisenträger et al. investigated the impact of the choice of the shape functions and element distortion on the condition number of the stiffness matrix [18]. Their study compared three high-order finite element methods (FEMs), i.e., the p -version of the FEM [19], the spectral element method (SEM) [20], and the NURBS-based IGA [1], by comparing numerical results with the condition number estimations from existing literature [21, 22, 23]. Gervasio et al. conducted a systematic comparison of the theoretical properties of SEM and NURBS-based IGA Galerkin methods for approximating the Poisson problem [24]. Their analysis focused on the convergence properties, algebraic structure, and spectral properties of the corresponding discrete systems. Additionally, the researchers proposed estimations for the behavior of the relevant theoretical laws with respect to design parameters such as mesh size, local degree, smoothness of NURBS basis functions, spatial dimension, and the *doF* involved in the computations.

For the IGA-C discretization matrices, Zampieri et al. analyzed the spectral properties of the mass and collocation matrices for specific acoustic wave problems, where they employed the IGA-C in space and the Newmark method in time [25]. However, a comprehensive study and estimation of the spectral properties of the IGA-L discretization matrices for standard PDEs is still lacking.

2. Preliminaries

2.1. B-spline and NURBS basis functions

Consider a set of distinct non-decreasing real numbers $\{\xi_0 = 0, \xi_1, \dots, \xi_{n-1}, \xi_n = 1\}$ in the one-dimensional patch $[0, 1]$, and given two positive integers p and k with $0 \leq k \leq p - 1$, let

$$\underbrace{\{\xi_0, \dots, \xi_0\}}_{p+1}, \underbrace{\{\xi_1, \dots, \xi_1\}}_{p-k}, \underbrace{\{\xi_{n-1}, \dots, \xi_{n-1}\}}_{p-k}, \underbrace{\{\xi_n, \dots, \xi_n\}}_{p+1} \quad (2)$$

be an open knot vector, i.e., the boundary knots have $p + 1$ multiplicity. The i -th univariate B-spline basis function $B_i^p(\xi)$ with the degree $p \geq 1$ and the regularity C^k can be defined over the above knot vector by means of the deBoor-Cox recursion formula [26]. The number of linear dependent basis functions is $N_b = (n - 1)(p - k) + p + 1$. In this paper, we utilize the uniform open knot vector, in which the internal knot values are uniformly distributed. Therefore, the mesh size $h = \frac{1}{n}$.

The regularity is a prominent property of B-splines, which denotes the global continuity of the basis functions. If internal knots are repeated $p - k$ times, then the B-splines are C^k -continuous, that stands for the *global order of regularity* [3].

In this paper, we consider two extreme values for k . When $k = p - 1$, the B-splines are globally C^{p-1} , and we use the notation $IGA - C^{p-1}$ to identify the case. When $k = 1$, we use the notation $IGA - C^1$.

In d -dimensional cases, the B-spline basis functions are calculated by tensor product. We introduce the parametric domain $\hat{\Omega} = [0, 1]^d$ with a knot vector (2) in each parametric direction. The multivariate B-spline basis on $\hat{\Omega}$ is $(B_{i_1}^{p_1} \cdots B_{i_d}^{p_d})$.

NURBS basis functions are defined starting from B-spline basis functions by associating a set of weights $\{\omega_1, \omega_2, \dots, \omega_{N_b}\}$. In this paper, we assume $\omega_i \in \mathbb{R}$, $\omega_i > 0$ for $i = 1, 2, \dots, N_b$. The i -th univariate NURBS basis function is

$$N_i^p(\xi) = \frac{\omega_i B_i^p(\xi)}{\sum_{j=1}^{N_b} \omega_j B_j^p(\xi)}. \quad (3)$$

NURBS inherit properties from their B-splines counterpart, so the degree of corresponding NURBS is p , and the global regularity is k .

2.2. Spectral properties estimations of IGA-G

The eigenvalues and the condition number of IGA-G matrices in Poisson equation have been systematically studied in [24]. Let $\mathbf{M} = (m_{ij})$ be the mass matrix, where

$$m_{ij} = (N_i^p, N_j^p) = \int_{\Omega} N_i^p N_j^p. \quad (4)$$

Let $\mathbf{K} = (k_{ij})$ be the stiffness matrix, where

$$k_{ij} = \int_{\Omega} \nabla N_i^p \cdot \nabla N_j^p. \quad (5)$$

The estimations in [24] show that for $k = 0$ regularity, it holds:

$$\begin{aligned}\lambda_{\min}(\mathbf{M}_0) &\sim h^d p^{-d/2} 4^{-pd} \\ \lambda_{\max}(\mathbf{M}_0) &\sim h^d p^{-d} \\ \mathcal{K}(\mathbf{M}_0) &\sim p^{-d/2} 4^{pd} \\ \lambda_{\min}(\mathbf{K}_0) &\sim \begin{cases} h^d p^{-d} & \text{if } h \lesssim (p^{2+d/2} 4^{-dp})^{1/2} \\ h^{d-2} p^{2-d/2} 4^{-dp} & \text{otherwise} \end{cases} \\ \lambda_{\max}(\mathbf{K}_0) &\sim h^{d-2} p^{2-d} \\ \mathcal{K}(\mathbf{K}_0) &\sim \begin{cases} h^{-2} p^2 & \text{if } h \lesssim (p^{2+d/2} 4^{-dp})^{1/2} \\ p^{-d/2} 4^{dp} & \text{otherwise} \end{cases}\end{aligned}\quad (6)$$

for $d = 1, 2, 3$, respectively. \mathbf{M}_0 represent the mass matrix and \mathbf{K}_0 is the stiffness matrix for $k = 0$ regularity. Let $\lambda_{\min}(\mathbf{M}_0)$, $\lambda_{\max}(\mathbf{M}_0)$ represent the minimum and maximum eigenvalues of \mathbf{M}_0 , respectively. The condition number of \mathbf{M}_0 is denoted by $\mathcal{K}(\mathbf{M}_0)$. The meanings of $\lambda_{\min}(\mathbf{K}_0)$, $\lambda_{\max}(\mathbf{K}_0)$ and $\mathcal{K}(\mathbf{K}_0)$ are analogous to those corresponding notations for \mathbf{M}_0 .

We denote with \mathbf{M}_{p-1} the mass matrix and \mathbf{K}_{p-1} the stiffness matrix associated with IGA- C^{p-1} approximation. For $k = p - 1$ regularity, it holds:

$$\begin{aligned}\lambda_{\min}(\mathbf{M}_{p-1}) &\sim \begin{cases} h^d e^{-pd} & \text{if } h \lesssim 1/p \\ \left(\frac{e}{4}\right)^{-d/h} \left(\frac{h}{p}\right)^{d/2} 4^{-pd} & \text{otherwise} \end{cases} \\ \lambda_{\max}(\mathbf{M}_{p-1}) &\sim \begin{cases} h^d & \text{if } h \lesssim 1/p \\ p^{-d} & \text{otherwise} \end{cases} \\ \mathcal{K}(\mathbf{M}_{p-1}) &\sim \begin{cases} e^{pd} & \text{if } h \lesssim 1/p \\ \left(\frac{e}{4}\right)^{d/h} (hp)^{-d/2} 4^{pd} & \text{otherwise} \end{cases}\end{aligned}$$

$$\lambda_{\min}(\mathbf{K}_{p-1}) \sim \begin{cases} h^d & \text{if } h \lesssim e^{-pd/2} \\ h^{d-2} e^{-pd} & \text{if } e^{-pd/2} \lesssim h \lesssim 1/p \\ (\frac{\epsilon}{4})^{-d/h} p^{2-d/2} h^{d/2} 4^{-pd} & \text{if } h \gtrsim 1/p \end{cases} \quad (7)$$

$$\lambda_{\max}(\mathbf{K}_{p-1}) \sim \begin{cases} ph^{d-2} & \text{if } h \lesssim 1/p \quad \text{for } p > 2 \\ p^{2-d} h^{-1} & \text{otherwise} \end{cases}$$

$$\mathcal{K}(\mathbf{K}_{p-1}) \sim \begin{cases} h^{-2} p & \text{if } h \lesssim e^{-pd/2} \\ pe^{dp} & \text{if } e^{-pd/2} \lesssim h \lesssim 1/p \\ (\frac{\epsilon}{4})^{d/h} p^{-d/2} h^{-d/2-1} 4^{dp} & \text{otherwise.} \end{cases}$$

In this paper, we study the spectral properties of the mass and collocation matrices arising in IGA-L for Poisson problems, and compare the numerical results with the estimations of IGA-G in the literature [24].

3. IGA-L discretization model

Let $\Omega \subset \mathbb{R}^d$, with $d = 1, 2, 3$, be a bounded domain, and let f be a given function. We consider the Poisson equation with homogeneous Dirichlet boundary conditions,

$$\begin{cases} -\Delta u = f & \text{in } \Omega \\ u = 0 & \text{on } \partial\Omega, \end{cases} \quad (8)$$

where u is the unknown solution. We discretize the strong form of the Poisson problem (8) using the least-squares collocation method of the isogeometric analysis with NURBS basis functions.

3.1. Isogeometric least-squares collocation method

In IGA, NURBS are used to represent both the computational domain $\Omega \subset \mathbb{R}^d$ and the numerical solution. The geometric mapping is derived by associating each basis function with a corresponding control point $\mathbf{P}_i \in \mathbb{R}^d$. Therefore, every point \mathbf{x} in the physical domain Ω can be expressed through the geometric mapping G ,

$$G : \mathbf{x}(\boldsymbol{\xi}) = \sum_{i=1}^{N_b} \mathbf{P}_i N_i^p(\boldsymbol{\xi}). \quad (9)$$

Assuming the geometric mapping is invertible, the mesh in the physical domain Ω can be uniquely determined by its corresponding mesh in the parameter domain $\hat{\Omega}$. The space of NURBS functions in the physical domain is defined as:

$$\mathcal{V}_{N_b} = \text{span} \{ N_i^p \circ G^{-1}, i = 1, \dots, N_b \}.$$

In two or higher dimensions, the space can be defined analogically:

$$\begin{aligned} \mathcal{V}_{N_i, N_j} &= \text{span} \{ N_{i,j}^{p,q} \circ G^{-1}, i = 1, \dots, N_i; j = 1, \dots, N_j \} \\ \mathcal{V}_{N_i, N_j, N_k} &= \text{span} \{ N_{i,j,k}^{p,q,r} \circ G^{-1}, i = 1, \dots, N_i; j = 1, \dots, N_j; \\ &\quad k = 1, \dots, N_k \}. \end{aligned}$$

IGA seeks the numerical solution to the problem (8) within the NURBS space incorporating the boundary conditions in the physical domain. The key idea behind IGA-L is to sample two sets of collocation points: $\{\tau_{j_1}^{in}, j_1 = 1, \dots, m^{in}\}$ in the interior of

the physical domain Ω , and $\{\tau_{j_2}^{bd}, j_2 = 1, \dots, m^{bd}\}$ on the boundary $\partial\Omega$. Thus, solving the IGA-L approximation of (8) is equivalent to finding the best approximation $U_h \in \mathcal{V}_{N_b}$ such that

$$\begin{cases} -\Delta U_h(\tau_{j_1}^{in}) = f(\tau_{j_1}^{in}) & j_1 = 1, \dots, m^{in} \\ U_h(\tau_{j_2}^{bd}) = 0 & j_2 = 1, \dots, m^{bd}. \end{cases} \quad (10)$$

The collocation points are determined based on the knot vectors. A commonly used set of collocation points is Greville abscissae [6]. Given a knot vector with regularity $k = p - 1$ as defined in (2), i.e.,

$$\underbrace{\{\xi_0, \dots, \xi_0, \xi_1, \dots, \xi_{n-1}, \xi_n, \dots, \xi_n\}}_{p+1},$$

we denote it as $\{\eta_0, \eta_1, \dots, \eta_{n+2p}\}$ for ease of presentation. The Greville abscissae points $\hat{\xi}_i, i = 0, 1, \dots, n + p - 1$ for classical IGA-C in the parameter domain are obtained by:

$$\hat{\xi}_i = \frac{\eta_{i+1} + \dots + \eta_{i+p}}{p}, \quad i = 0, \dots, n + p - 1. \quad (11)$$

The corresponding collocation points in the physical domain are obtained through the geometric mapping (9): $\tau_i = x(\hat{\xi}_i)$. Let m denotes the total number of collocation points in IGA-L. To generate these m points, a knot vector of size $m + p + 1$ with regularity $k = p - 1$ is constructed, i.e.,

$$\underbrace{\{\xi_0, \dots, \xi_0, \xi_1, \dots, \xi_{m-p-1}, \xi_{m-p}, \dots, \xi_{m-p}\}}_{p+1},$$

which can be denoted as $\{\eta_0, \eta_1, \dots, \eta_{m+p}\}$. The Greville abscissae points are then calculated as follows:

$$\hat{\xi}_i = \frac{\eta_{i+1} + \dots + \eta_{i+p}}{p}, \quad i = 0, \dots, m - 1. \quad (12)$$

The collocation points in the physical domain are given by the geometric mapping (9): $\tau_i = x(\hat{\xi}_i)$.

SC points are developed based on the superconvergent theory. Anitescu et al. aimed to identify collocation points where the numerical solution exhibits behavior similar to that of the standard Galerkin solution [9]. Table 1 presents the locations of superconvergent points within the reference interval $[-1, 1]$ for different degrees. These SC points are obtained by mapping the superconvergent points from the reference interval to the knot interval $[\xi_i, \xi_{i+1}]$. Since the number of superconvergent points is approximately twice the number of *dof*, and all these points are utilized, IGA-C with SC points naturally leads to the formation of a least-squares system.

Table 1: Superconvergent points in the reference interval.

Degree	Superconvergent Points
$p = 3$	$-\frac{1}{\sqrt{3}}, \frac{1}{\sqrt{3}}$
$p = 4$	$-1, 0, 1$
$p = 5$	$-\frac{\sqrt{225-30\sqrt{3}}}{15}, \frac{\sqrt{225-30\sqrt{3}}}{15}$
$p = 6$	$-1, 0, 1$
$p = 7$	$-0.50491856751, 0.50491856751$

CG points are selected as a specific subset of the superconvergent points [12]. They retain one superconvergent point in each

knot interval while maintaining global symmetry. As a result, the number of CG points equals the number of *dof*. Fig.1 shows the distribution of Greville points, SC points and CG points when the degree $p = 3$.

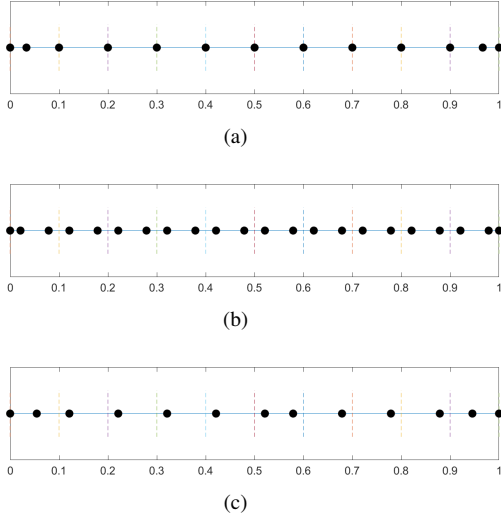


Fig. 1. Distributions of different types of collocation points ($p = 3$). (a) Greville points. (b) SC points. (c) CG points.

3.2. Matrix form of IGA-L

In IGA, the numerical solution U_h is defined on a mesh determined by the geometric mapping. Consequently, U_h in IGA is represented as a linear combination of the NURBS basis functions in Ω , which also serve as the basis functions for the geometric mapping G .

For one-dimensional problems, the numerical solution can be expressed as:

$$U_h(\tau) = \sum_{i=1}^{N_b} u_i N_{i,p}(G^{-1}(\tau)), \quad \tau \in \Omega \quad (13)$$

where $\{u_i\}_{i=1}^{N_b}$ are the unknown control coefficients. By substituting (13) to (10) we obtain a non-symmetric linear system with respect to the unknowns $\{u_i\}_{i=1}^{N_b}$. The vector $\{u_i\}_{i=1}^{N_b}$ is arranged into a column vector, and the basis functions and collocation points are reordered such that the first N_b^{in} basis functions correspond to the internal control coefficients, and the first m^{in} collocation points lie within the support of the internal basis functions.

We define $\mathbf{u} = [u_i]_{i=1}^{N_b^{in}}$, and $\mathbf{b} = [f(\tau_j)]_{j=1}^{m^{in}}$. Thus, the problem (10) can be reformulated in a matrix form as:

$$\mathbf{A}\mathbf{u} = \mathbf{b} \quad (14)$$

with

$$\begin{aligned} \mathbf{A}_{ji} &= -\Delta N_{i,p}(G^{-1}(\tau_j)) \quad j = 1, \dots, m^{in}; \quad i = 1, \dots, N_b^{in}, \\ \mathbf{b}_j &= f(\tau_j) \quad j = 1, \dots, m^{in}. \end{aligned}$$

\mathbf{A} denotes the *collocation matrix* with m^{in} rows and N_b^{in} columns, and \mathbf{b} is the *load vector*. The *mass matrix* \mathbf{M} in IGA-L is defined as a collocation matrix on the basis functions directly:

$$\mathbf{M}_{ji} = N_{i,p}(G^{-1}(\tau_j)) \quad j = 1, \dots, m^{in}; \quad i = 1, \dots, N_b^{in}. \quad (15)$$

The numerical solution is then obtained by solving the least-squares linear system (14). The corresponding least-squares problem is given by:

$$\min_{\mathbf{u}} \|\mathbf{A}\mathbf{u} - \mathbf{b}\|^2. \quad (16)$$

The normal equations associated with (16) are:

$$\mathbf{A}^T \mathbf{A} \mathbf{u} = \mathbf{A}^T \mathbf{b}. \quad (17)$$

4. Numerical analysis

In this section, we analyze the condition number and singular values of the collocation and mass matrices in IGA-L model for the Poisson problem with homogeneous Dirichlet boundary conditions.

For any matrix \mathbf{A} (which may not be square), let $\sigma_{max}(\mathbf{A})$ and $\sigma_{min}(\mathbf{A})$ denote its maximum and minimum singular values, respectively. The *spectral condition number* of \mathbf{A} is given by:

$$\mathcal{K}(\mathbf{A}) = \frac{\sigma_{max}(\mathbf{A})}{\sigma_{min}(\mathbf{A})}. \quad (18)$$

The spectral condition number of the matrix \mathbf{A} increases as its columns or rows become more unevenly distributed or closer to linear dependence. The former tends to increase $\sigma_{max}(\mathbf{A})$, while the latter tends to decrease $\sigma_{min}(\mathbf{A})$.

Based on Section 3, we summarize the factors affecting the spectral properties of the collocation and mass matrices in IGA-L as follows:

- The type of partial differential equations, including the differential operators and the boundary conditions.
- Geometric mapping, i.e., the parameterization of the physical domain.
- Dimension d .
- Degree p of the NURBS basis functions.
- Mesh size h .
- Regularity k .
- Number of collocation points m .
- Distribution of collocation points.

For the numerical analysis, we primarily focus on the effects of the degree p , mesh size h , regularity k , dimension d , as well as the number and distribution of collocation points on the spectral properties of the collocation and mass matrices. We present estimates for the condition number and singular values of IGA-L matrices with respect to h and p , and explore how the number and distribution of the collocation points influence these properties.

We consider the Poisson problem in one-, two-, and three-dimensional physical domains. The one-dimensional physical domain is $\Omega = [0, 1]$. The two-dimensional physical domain is a quarter of the annulus, and for the three-dimensional case, we study a unit cube $\Omega = [0, 1]^3$ and a model of 1/8th of a hollow sphere. The radius of the mid-surface of the hollow sphere is 10 and the thickness of the model is 0.04. Fig. 2 shows the two- and three-dimensional physical domains we study in this paper.

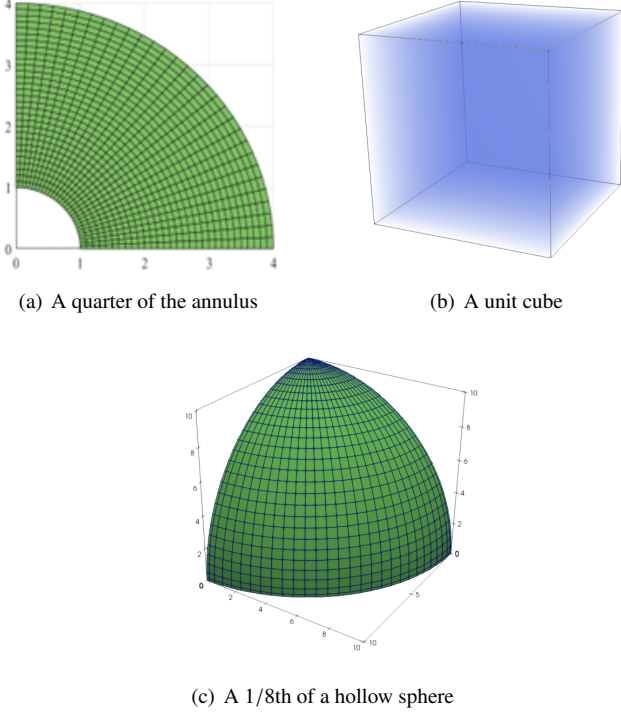


Fig. 2. Physical domain in two- and three-dimensional cases.

For the regularity, we consider two cases: $k = p-1$ (denoted as $IGA-C^{p-1}$) and $k = 1$ (denoted as $IGA-C^1$). The corresponding collocation matrices are denoted as \mathbf{A}_{p-1} and \mathbf{A}_1 , respectively. Similarly, the mass matrices for these two cases are denoted as \mathbf{M}_{p-1} and \mathbf{M}_1 , respectively.

Due to RAM and memory limitations, the ranges of p and h vary depending on the regularity and the spatial dimension. For the distribution of collocation points, we consider the Greville points, SC points and CG points. We first focus on the Greville points in the following analysis, where the number of collocation points is initially set to four times the *dof*. We summarize the main results, conduct numerical analysis of both the collocation matrix and the mass matrix in IGA-L, and present estimations for their condition number and singular values in relation to p , h and k . All the experiments are conducted on a PC with an Intel Core i7-10700 2.90GHz CPU and 16GB of RAM.

4.1. $IGA-C^{p-1}$ collocation matrix

In this section, we study the spectral properties of the $IGA-C^{p-1}$ collocation matrix \mathbf{A}_{p-1} . The mesh size h ranges from 0.1 to 0.01, with a decrease from 0.2 to 0.05 when $d = 3$. The degree p starts at 2, and increases to 24, 16, 7 for $d = 1, 2, 3$, respectively. For the hollow sphere model, the mesh size ranges from 0.1 to 0.05, and the degree p starts at 4 and increases to 7.

The numerical results show that for $h > 0$, $p \geq 2$ and $d = 1, 2, 3$, $\sigma_{min}(\mathbf{A}_{p-1})$, $\sigma_{max}(\mathbf{A}_{p-1})$ and $\mathcal{K}(\mathbf{A}_{p-1})$ behave as:

$$\sigma_{min}(\mathbf{A}_{p-1}) \sim \begin{cases} c_1 & \text{if } h \lesssim e^{-pd/4} p^{d/8} \\ (e/2)^{-2dp} p^{(4/e)^d} h^{-2} & \text{otherwise,} \end{cases} \quad (19)$$

$$\sigma_{max}(\mathbf{A}_{p-1}) \sim h^{-2} p^2, \quad (20)$$

$$\mathcal{K}(\mathbf{A}_{p-1}) \sim \begin{cases} h^{-2} p^2 & \text{if } h \lesssim e^{-pd/4} p^{d/8} \\ (e/2)^{2dp} p^{2-(4/e)^d} & \text{otherwise,} \end{cases} \quad (21)$$

where c_1 is independent of h and p . The symbol \sim means "up to a constant independent of both h and p ".

In Figs.3, 4, 5 and 6, we demonstrate the $\mathcal{K}(\mathbf{A}_{p-1})$, $\sigma_{max}(\mathbf{A}_{p-1})$ and $\sigma_{min}(\mathbf{A}_{p-1})$ versus h (at left) and p (at right) for $d = 1, 2, 3$. As shown in Figs. 3(a), 4(a), 5(a) and 6(a), $\mathcal{K}(\mathbf{A}_{p-1})$ increases at a rate of about h^{-2} . In Fig. 6(a), $\mathcal{K}(\mathbf{A}_{p-1})$ tends to grow at a slightly higher rate than h^{-2} in a case for small h . Figs. 3(b), 4(b), 5(b) and 6(b) show that $\mathcal{K}(\mathbf{A}_{p-1})$ increases at a rate of about $p^{2-(4/e)^d} (e/2)^{2dp}$, which is essentially in line with our estimates. Numerical results show that the condition number of \mathbf{A}_{p-1} with respect to p basically satisfies $\mathcal{K}(\mathbf{A}_{p-1}) \sim h^{-2} p^2$ when $h \lesssim e^{-pd/4} p^{d/8}$. Additionally, when $h \gtrsim e^{-pd/4} p^{d/8}$, the condition number grows exponentially with p and tends to be stable with h -refinement, which is due to the increase in the minimum singular value at this time.

As for the maximum singular value $\sigma_{max}(\mathbf{A}_{p-1})$, Figs.3(c), 4(c), 5(c) and 6(c) show that $\sigma_{max}(\mathbf{A}_{p-1})$ increases at a rate of about h^{-2} with h -refinement for any value of $p \geq 2$. Figs.3(d), 4(d), 5(d) and 6(d) illustrate a growth rate of about p^2 for any value of $h > 0$. However, in Fig. 6(c), it can be observed that for the hollow sphere example, the maximum singular value $\sigma_{max}(\mathbf{A}_{p-1})$ initially increases at a rate of about h^{-2} with h -refinement. In a case for small h , $\sigma_{max}(\mathbf{A}_{p-1})$ exhibits a growth rate slightly higher than h^{-2} . Moreover, Fig. 6(d) demonstrates that as p increases, the growth rate of $\sigma_{max}(\mathbf{A}_{p-1})$ is slightly higher than p^2 .

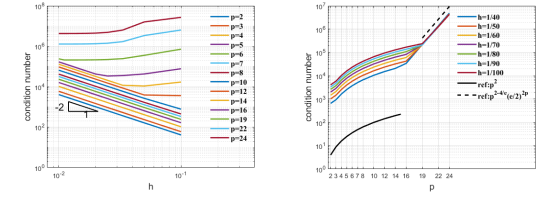
Regarding $\sigma_{min}(\mathbf{A}_{p-1})$, it initially increases by h^{-2} , then stabilizes with further h -refinement. As p increases, the mesh size h required for $\sigma_{min}(\mathbf{A}_{p-1})$ to remain stable becomes smaller. Fig.3(e) shows that for $p = 12$, the breakpoint for h lies between 0.05 and 0.1, while for $p = 14$, it lies between 0.033 and 0.05. The numerical results about $\sigma_{min}(\mathbf{A}_{p-1})$ show that $\sigma_{min}(\mathbf{A}_{p-1})$ remains independent of h and p when $h \lesssim e^{-pd/4} p^{d/8}$. When h is relatively large, the support interval of the basis functions can no longer be completely contained within the parameter domain. This affects the linear independence of the column vectors of \mathbf{A}_{p-1} , leading to an increase in $\sigma_{min}(\mathbf{A}_{p-1})$ with h -refinement and a decrease of about $(e/2)^{-2dp} p^{(4/e)^d}$ as p increases. For the hollow sphere example, Fig. 6(e) shows that $\sigma_{min}(\mathbf{A}_{p-1})$ tends to be stable with h -refinement. Fig. 6(f) shows as p increases, $\sigma_{min}(\mathbf{A}_{p-1})$ decreases by about $(e/2)^{-6p} p^{(4/e)^3}$, which is basically consistent with our estimates.

As shown in Fig. 6, the numerical results of the collocation matrix for the hollow sphere example deviate slightly from our estimates, which may be due to different geometric mappings. However, in general, the results are basically in line with our estimates, which suggests that the spectral properties of the collocation matrix behave approximately the same under different geometric mappings.

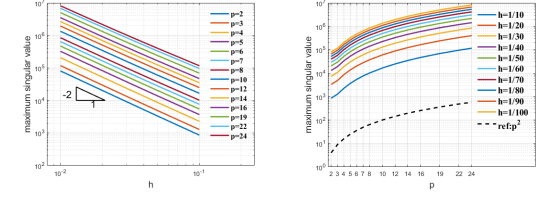
According to (21) and (7), it can be observed that when $h \lesssim e^{-pd/2}$, the stiffness matrix \mathbf{K}_{p-1} in IGA-G is slightly better conditioned than the collocation matrix in IGA-L. However, this condition on h is quite stringent in practice. When $h \gtrsim e^{-pd/4} p^{d/8}$, the condition number of the collocation matrix satisfies $\mathcal{K}(\mathbf{A}_{p-1}) \sim (e/2)^{2dp} p^{2-(4/e)^d}$, which is much better conditioned than \mathbf{K}_{p-1} .

4.2. $IGA-C^{p-1}$ mass matrix

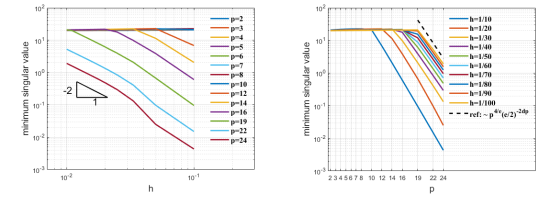
In this section, we study the spectral properties of the $IGA-C^{p-1}$ mass matrix \mathbf{M}_{p-1} . The mesh size h and the degree p are set to be the same as those used in the previous section. The



(a) Condition number vs. h (b) Condition number vs. p

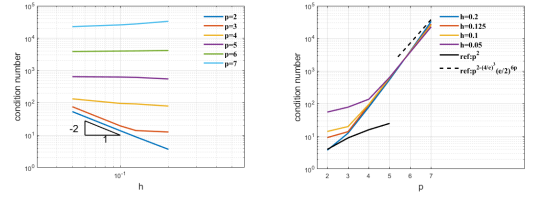


(c) Maximum singular value vs. h (d) Maximum singular value vs. p

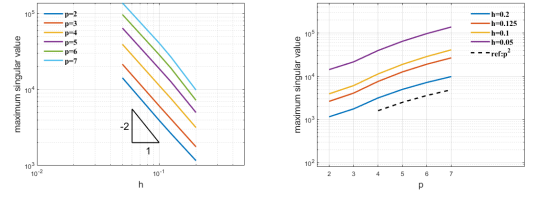


(e) Minimum singular value vs. h (f) Minimum singular value vs. p

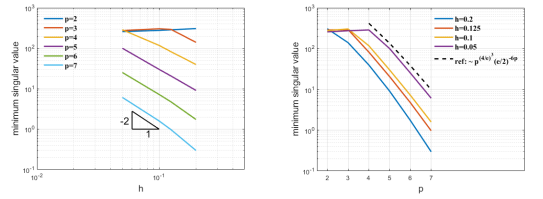
Fig. 3. The maximum/minimum singular value and the spectral condition number of $\mathcal{K}(A_{p-1})$ for $d = 1$, versus h (at left) and versus p (at right).



(a) Condition number vs. h (b) Condition number vs. p

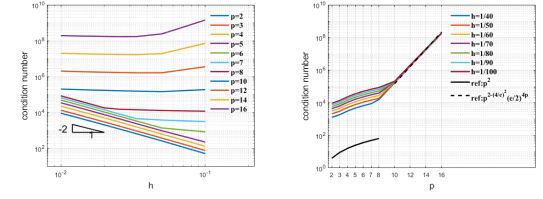


(c) Maximum singular value vs. h (d) Maximum singular value vs. p

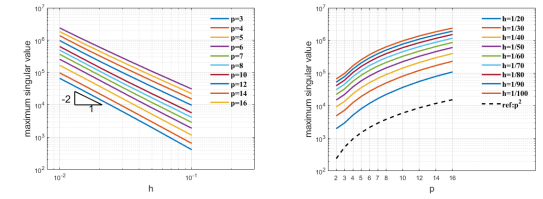


(e) Minimum singular value vs. h (f) Minimum singular value vs. p

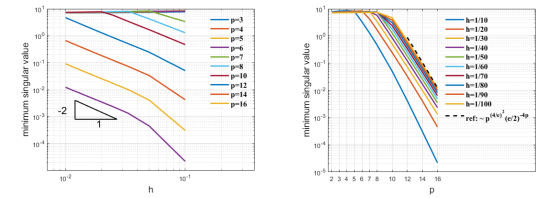
Fig. 5. The maximum/minimum singular value and the spectral condition number of $\mathcal{K}(A_{p-1})$ for a cube example, versus h (at left) and versus p (at right).



(a) Condition number vs. h (b) Condition number vs. p

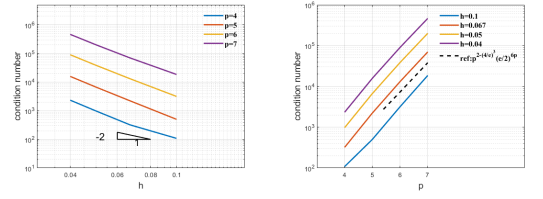


(c) Maximum singular value vs. h (d) Maximum singular value vs. p

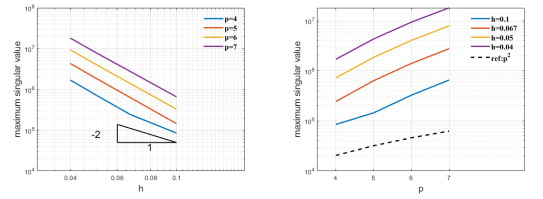


(e) Minimum singular value vs. h (f) Minimum singular value vs. p

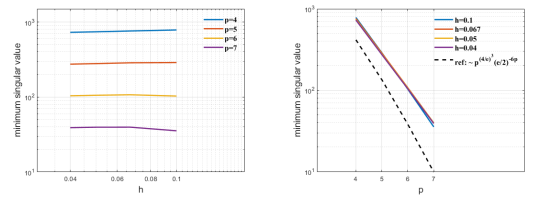
Fig. 4. The maximum/minimum singular value and the spectral condition number of $\mathcal{K}(A_{p-1})$ for $d = 2$, versus h (at left) and versus p (at right).



(a) Condition number vs. h (b) Condition number vs. p



(c) Maximum singular value vs. h (d) Maximum singular value vs. p



(e) Minimum singular value vs. h (f) Minimum singular value vs. p

Fig. 6. The maximum/minimum singular value and the spectral condition number of $\mathcal{K}(A_{p-1})$ for 1/8th of hollow sphere, versus h (at left) and versus p (at right).

numerical results show that for $h > 0$, $p \geq 2$ and $d = 1, 2, 3$, $\sigma_{\min}(\mathbf{M}_{p-1})$, $\sigma_{\max}(\mathbf{M}_{p-1})$ and $\mathcal{K}(\mathbf{M}_{p-1})$ behave as:

$$\sigma_{\min}(\mathbf{M}_{p-1}) \sim e^{-dp/2} \quad (22)$$

$$\sigma_{\max}(\mathbf{M}_{p-1}) \sim c_2, \quad (23)$$

$$\mathcal{K}(\mathbf{M}_{p-1}) \sim e^{dp/2} \quad (24)$$

where c_2 is independent of h and p .

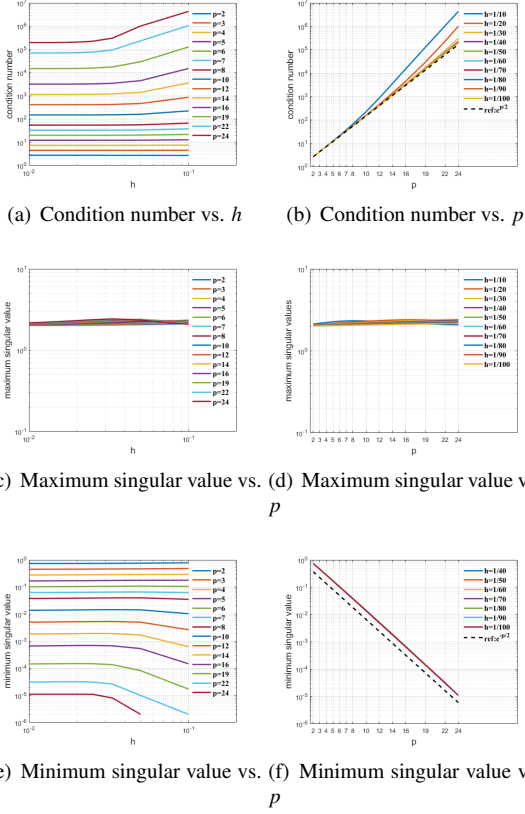


Fig. 7. The maximum/minimum singular value and the spectral condition number of $\mathcal{K}(\mathbf{M}_{p-1})$ for $d = 1$, versus h (at left) and versus p (at right).

In Figs. 7, 8, 9 and 10, we show the $\mathcal{K}(\mathbf{M}_{p-1})$, $\sigma_{\max}(\mathbf{M}_{p-1})$ and $\sigma_{\min}(\mathbf{M}_{p-1})$ versus h (at left) and p (at right) for $d = 1, 2, 3$. For the condition number $\mathcal{K}(\mathbf{M}_{p-1})$, Figs. 7(a), 8(a), 9(a) and 10(a) demonstrate that $\mathcal{K}(\mathbf{M}_{p-1})$ does not vary with h when h is relatively small. Figs. 7(b), 8(b) and 9(b) show that for $d = 1$, $\mathcal{K}(\mathbf{M}_{p-1})$ increases by about $e^{p/2}$; for $d = 2$, it increases as e^p ; and for $d = 3$, it increases by about $e^{3p/2}$. However, Fig. 10(b) demonstrates that for the hollow sphere example, the growth rate of $\mathcal{K}(\mathbf{M}_{p-1})$ is slightly lower than $e^{3p/2}$. For the maximum singular value $\sigma_{\max}(\mathbf{M}_{p-1})$, numerical results demonstrate that $\sigma_{\max}(\mathbf{M}_{p-1})$ is independent of both h and p for $h > 0$ and $p \geq 2$. This is due to the relatively uniform distribution of the columns of the mass matrix formed by the internal NURBS basis functions.

As shown in Figs. 7(e), 8(e), 9(e) and 10(e), the minimum singular value of the mass matrix $\sigma_{\min}(\mathbf{M}_{p-1})$ essentially does not change with h -refinement. In Fig. 7(e), it can be observed that for relatively large degrees p , $\sigma_{\min}(\mathbf{M}_{p-1})$ initially increases with h -refinement, and then remains constant. Figs. 7(f), 8(f), 9(f) and 10(f) show that as p increases, $\sigma_{\min}(\mathbf{M}_{p-1})$ decreases exponentially with p . When $d = 1$, $\sigma_{\min}(\mathbf{M}_{p-1})$ decreases by about

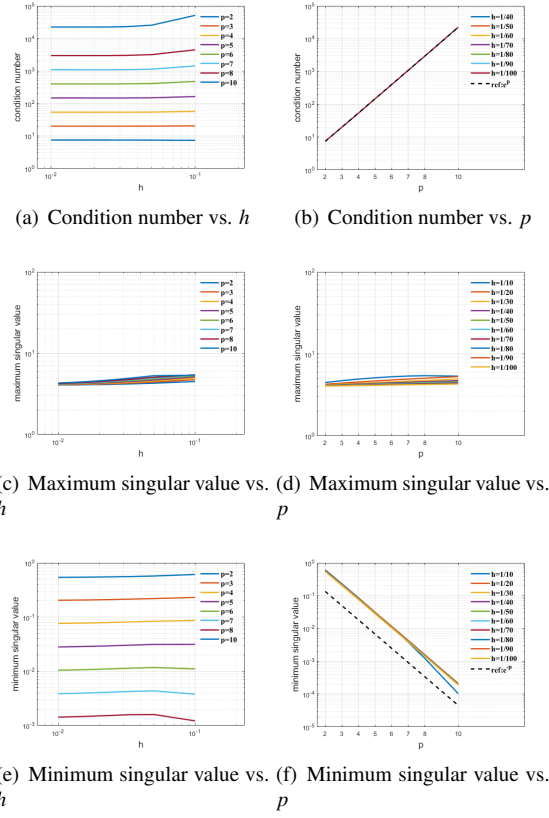


Fig. 8. The maximum/minimum singular value and the spectral condition number of $\mathcal{K}(\mathbf{M}_{p-1})$ for $d = 2$, versus h (at left) and versus p (at right).

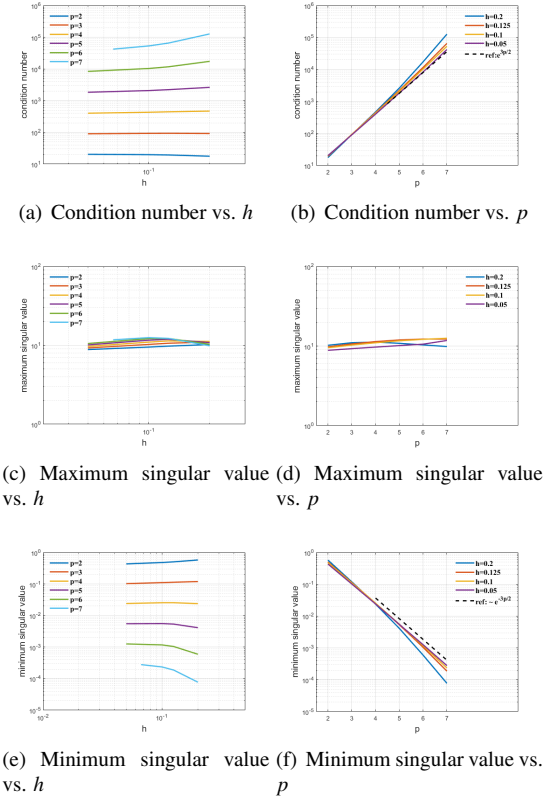


Fig. 9. The maximum/minimum singular value and the spectral condition number of $\mathcal{K}(\mathbf{M}_{p-1})$ for a cube example, versus h (at left) and versus p (at right).

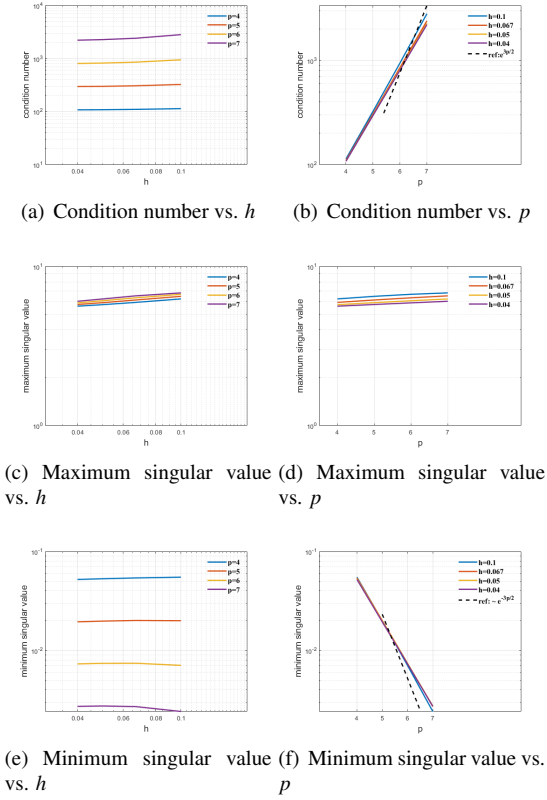


Fig. 10. The maximum/minimum singular value and the spectral condition number of $\mathcal{K}(\mathbf{M}_{p-1})$ for 1/8th of hollow sphere, versus h (at left) and versus p (at right).

$e^{-p/2}$ as p ; when $d = 2$, it decreases as e^{-p} ; and when $d = 3$, it decreases by about $e^{-3p/2}$. Moreover, Fig. 10(f) shows that for the hollow sphere example, $\sigma_{\min}(\mathbf{M}_{p-1})$ decreases slightly slower than $e^{-3p/2}$. In general, the numerical results shown in Figs.7, 8, 9 and 10 are basically in line with our estimates (22)- (24). Compared with the condition number estimations of \mathbf{M}_{p-1} in IGA-G (7), we find that \mathbf{M}_{p-1} in IGA-L is better conditioned for any value $h > 0$.

4.3. IGA- C^1 collocation matrix

In this section, we study the spectral properties of the IGA- C^1 collocation matrix \mathbf{A}_1 . The mesh size h varies from 0.1 to 0.01 for $d = 1$. For $d = 2$, h is set to decrease from 0.2 to 0.05. For $d = 3$, h is set to decrease from 0.2 to 0.1. The degree p starts at 2, and increases to 16, 7, 4 for $d = 1, 2, 3$, respectively.

The numerical results show that for $h > 0$, $p \geq 2$ and $d = 1, 2, 3$, $\sigma_{\min}(\mathbf{A}_1)$, $\sigma_{\max}(\mathbf{A}_1)$ and $\mathcal{K}(\mathbf{A}_1)$ behave as:

$$\sigma_{\min}(\mathbf{A}_1) \sim c_3 \quad (25)$$

$$\sigma_{\max}(\mathbf{A}_1) \sim h^{-2} p^{5/2} \quad (26)$$

$$\mathcal{K}(\mathbf{A}_1) \sim h^{-2} p^{5/2} \quad (27)$$

where c_3 is independent of h and p .

Figs.11(c), 12(c) and 13(c) demonstrate that $\sigma_{\max}(\mathbf{A}_1)$ grows as h^{-2} with h -refinement. Moreover, Figs.11(d), 12(d) and 13(d) show that $\sigma_{\max}(\mathbf{A}_1)$ grows approximately as $p^{2.5}$ with p -refinement. Thus, we obtain the estimate $\sigma_{\max}(\mathbf{A}_1) \sim h^{-2} p^{2.5}$.

Figs.11(e), 12(e) and 13(e) show that $\sigma_{\min}(\mathbf{A}_1)$ is independent of h for any value $p \geq 2$. Additionally, Figs.11(f), 12(f) and

13(f) demonstrate that $\sigma_{\min}(\mathbf{A}_1)$ is also independent of p . Thus, we obtain the estimate of the condition number $\mathcal{K}(\mathbf{A}_1) \sim h^{-2} p^{2.5}$. The numerical results shown in Figs.11, 12 and 13 confirm our estimations (25)- (27).

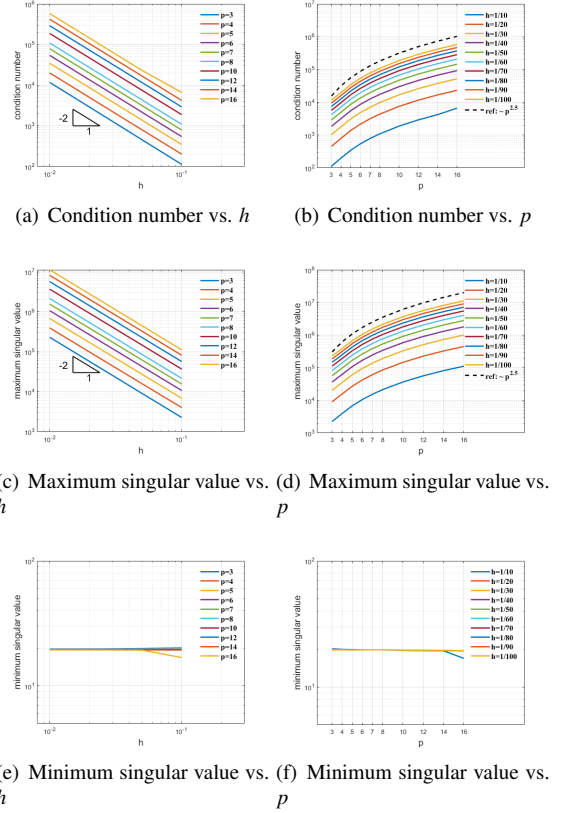


Fig. 11. The maximum/minimum singular value and the spectral condition number of $\mathcal{K}(\mathbf{A}_1)$ for $d = 1$, versus h (at left) and versus p (at right).

4.4. IGA- C^1 mass matrix

In this section, we study the spectral properties of the IGA- C^1 mass matrix \mathbf{M}_1 . The mesh size h and the degree p are set to be the same as those used in the previous section. The numerical results show that for $h > 0$, $p \geq 2$ and $d = 1, 2, 3$, $\sigma_{\min}(\mathbf{M}_1)$, $\sigma_{\max}(\mathbf{M}_1)$ and $\mathcal{K}(\mathbf{M}_1)$ behave as:

$$\sigma_{\min}(\mathbf{M}_1) \sim (2d)^{-p} \quad (28)$$

$$\sigma_{\max}(\mathbf{M}_1) \sim c_4 \quad (29)$$

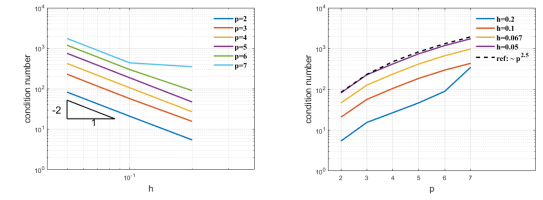
$$\mathcal{K}(\mathbf{M}_1) \sim (2d)^p \quad (30)$$

where c_4 is independent of h and p .

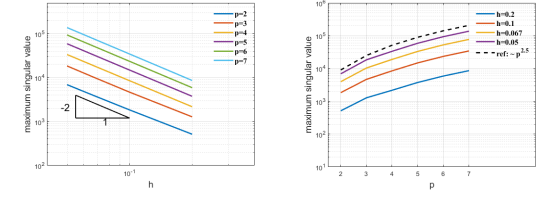
Figs.14(c), 15(c) and 16(c) show that $\sigma_{\max}(\mathbf{M}_1)$ is independent of both h and p for $h > 0$ and $p \geq 2$. In Figs.14-16 we observe that $\sigma_{\min}(\mathbf{M}_1)$ and $\mathcal{K}(\mathbf{M}_1)$ are also independent of h . For p -refinement, the minimum singular value $\sigma_{\min}(\mathbf{M}_1)$ decreases exponentially with p . Specifically, for $d = 1$, $\sigma_{\min}(\mathbf{M}_1)$ decreases by about 2^{-p} ; for $d = 2$, it decreases by about 4^{-p} ; and for $d = 3$, it decreases by about 6^{-p} . Thus, we obtain the estimations $\sigma_{\min}(\mathbf{M}_1) \sim (2d)^{-p}$ and $\mathcal{K}(\mathbf{M}_1) \sim (2d)^p$.

4.5. Sparsity pattern

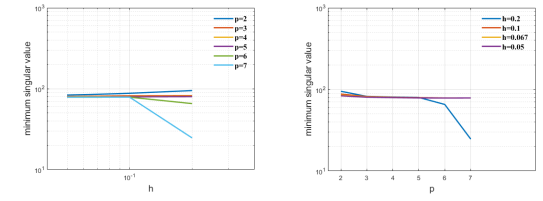
It is well known that the number of non-zero entries of the collocation matrix is a measure not only of the memory space



(a) Condition number vs. h (b) Condition number vs. p

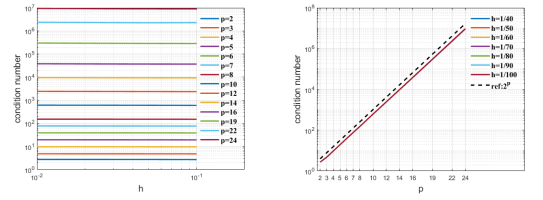


(c) Maximum singular value vs. h (d) Maximum singular value vs. p

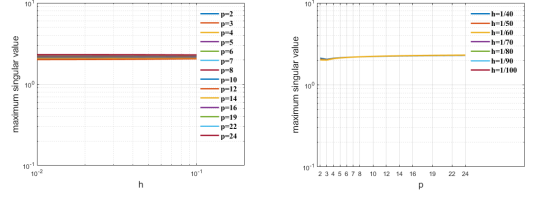


(e) Minimum singular value vs. h (f) Minimum singular value vs. p

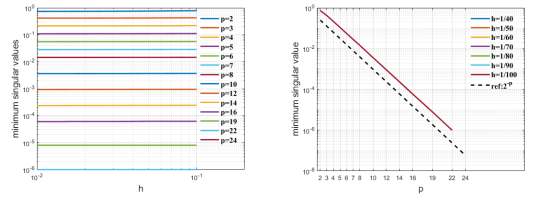
Fig. 12. The maximum/minimum singular value and the spectral condition number of $\mathcal{K}(\mathbf{A}_1)$ for $d = 2$, versus h (at left) and versus p (at right).



(a) Condition number vs. h (b) Condition number vs. p

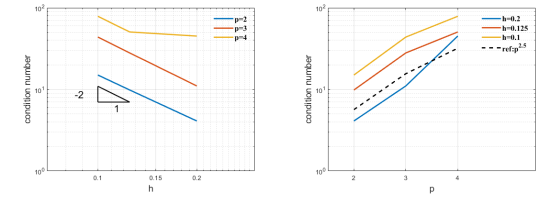


(c) Maximum singular value vs. h (d) Maximum singular value vs. p

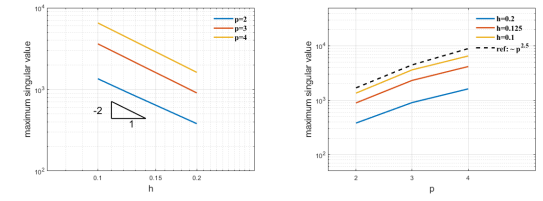


(e) Minimum singular value vs. h (f) Minimum singular value vs. p

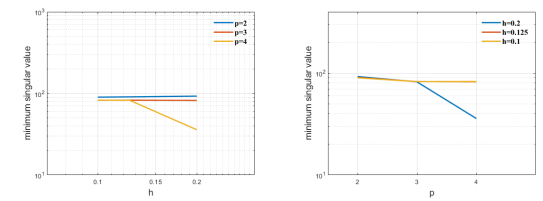
Fig. 14. The maximum/minimum singular value and the spectral condition number of $\mathcal{K}(\mathbf{M}_1)$ for $d = 1$, versus h (at left) and versus p (at right).



(a) Condition number vs. h (b) Condition number vs. p

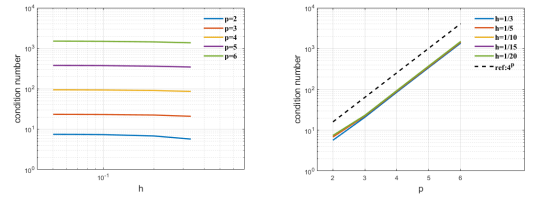


(c) Maximum singular value vs. h (d) Maximum singular value vs. p

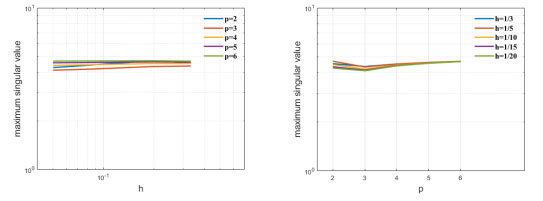


(e) Minimum singular value vs. h (f) Minimum singular value vs. p

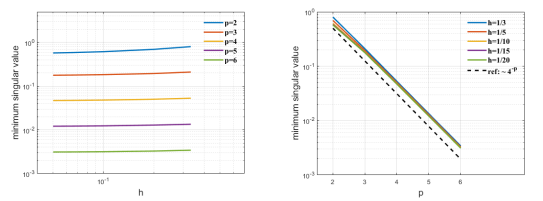
Fig. 13. The maximum/minimum singular value and the spectral condition number of $\mathcal{K}(\mathbf{A}_1)$ for $d = 3$, versus h (at left) and versus p (at right).



(a) Condition number vs. h (b) Condition number vs. p



(c) Maximum singular value vs. h (d) Maximum singular value vs. p



(e) Minimum singular value vs. h (f) Minimum singular value vs. p

Fig. 15. The maximum/minimum singular value and the spectral condition number of $\mathcal{K}(\mathbf{M}_1)$ for $d = 2$, versus h (at left) and versus p (at right).

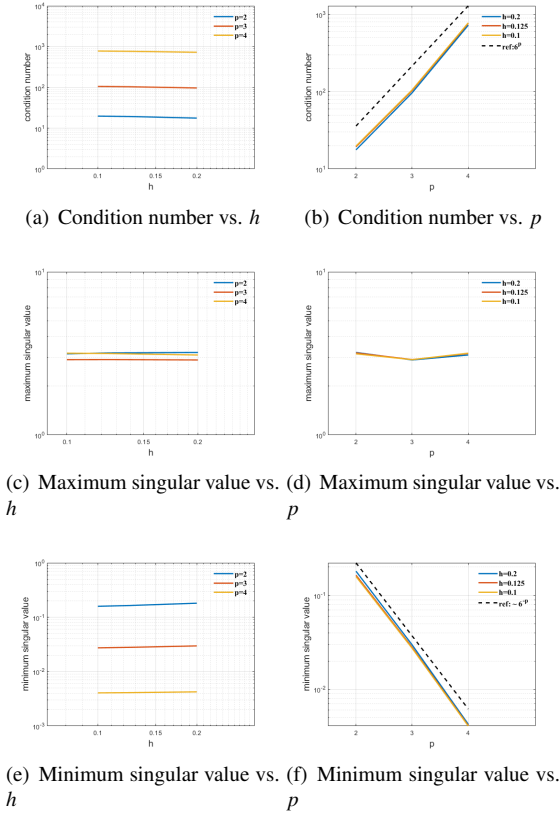


Fig. 16. The maximum/minimum singular value and the spectral condition number of $\mathcal{K}(\mathbf{M}_1)$ for $d = 3$, versus h (at left) and versus p (at right).

required to store the matrix, but also of the computational complexity involved in assembling the collocation matrix and solving the linear system. In this section, we analyze the sparsity patterns of $\mathbf{A}^T \mathbf{A}$ for regularity $k = 1$ and $k = p - 1$, with three values of degree $p = 4, 8, 12$ and three values of mesh size $h = 0.2, 0.1, 0.067$ in two-dimensional case. Here, \mathbf{A} denotes the collocation matrix in IGA-L.

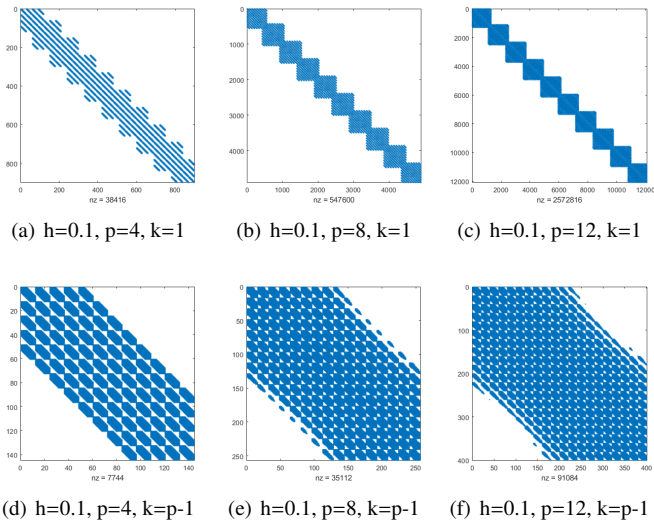


Fig. 17. The sparsity pattern of $\mathbf{A}^T \mathbf{A}$ for a fixed mesh size $h = 0.1$.

In Fig.17, we illustrate the sparsity patterns of $\mathbf{A}^T \mathbf{A}$ for regu-

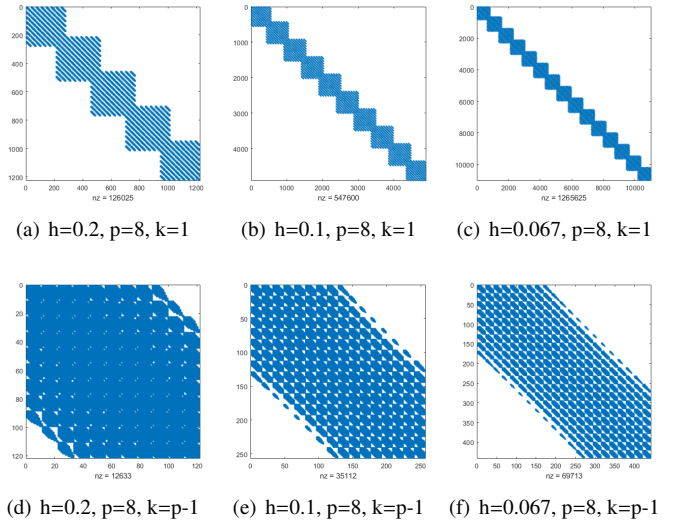


Fig. 18. The sparsity pattern of $\mathbf{A}^T \mathbf{A}$ for a fixed degree $p = 8$.

larity $k = 1$ (top), $k = p - 1$ (bottom), with three values of degree $p = 4$ (left), $p = 8$ (center) and $p = 12$ (right) for a fixed mesh size $h = 0.1$. We observe that the number of non-zero entries in $\mathbf{A}^T \mathbf{A}$ increases as p increases. Additionally, $\mathbf{A}^T \mathbf{A}$ becomes considerably denser as the regularity increases.

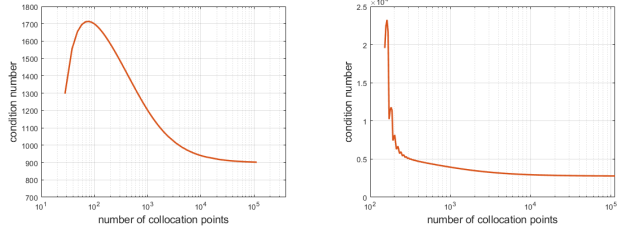
Fig.18 shows the sparsity patterns of $\mathbf{A}^T \mathbf{A}$ for regularity $k = 1$ (top), $k = p - 1$ (bottom), with three values of mesh size $h = 0.2$ (left), $h = 0.1$ (center) and $h = 0.067$ (right) for a fixed degree $p = 8$. We observe that the number of non-zero entries in $\mathbf{A}^T \mathbf{A}$ increases as h decreases. Compared to IGA-C, the collocation matrix in IGA-L is slightly denser for the same parameters. For example, when $h = 0.2$, $p = 8$, and $k = 1$, the number of non-zero entries in the collocation matrix of IGA-C is 100,489, whereas in IGA-L it is 126,025 [25].

4.6. Collocation point

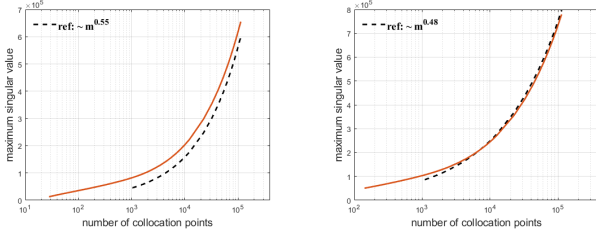
In this section, we analyze the effect of the number and the distribution of the collocation points on the spectral properties of the collocation matrix. The degree p is fixed at 8, and the mesh size is set to $h = 0.05$. We conduct experiments in one-dimensional case, with the number of collocation points initially set to be equal to the *dof*.

Fig.19 shows the condition number (top), maximum singular value (center) and minimum singular value (bottom) as the number of collocation points m increases for $k = p - 1$ (left) and $k = 1$ (right). In Figs.19(a) and 19(b) we observe that as the number of collocation points increases, $\mathcal{K}(\mathbf{A})$ initially increases, then decreases, and finally stabilizes. When the number of collocation points significantly exceeds the number of *dof*, $\mathcal{K}(\mathbf{A})$ can be much lower than that in IGA-C. For $k = 1$ regularity, the condition number decreases more rapidly than for $k = p - 1$ as the number of collocation points increases, suggesting that in the IGA-L method with $k = 1$ regularity, using slightly more collocation points than the *dof* can lead to a better-conditioned linear system compared to IGA-C.

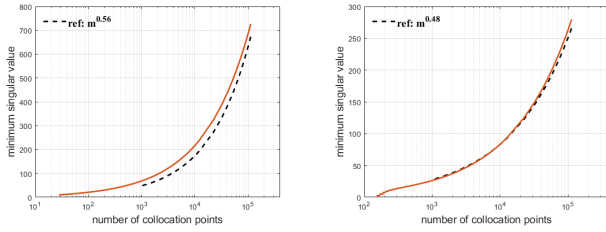
From Figs.19(c) and 19(d) we observe that as the number of collocation points increases, $\sigma_{\max}(\mathbf{A}_{p-1}) \sim m^{0.55}$ and $\sigma_{\max}(\mathbf{A}_1) \sim m^{0.48}$, indicating that the maximum singular value for $k = p - 1$ regularity increases more rapidly than for $k = 1$. Similarly, Figs.19(c) and 19(d) show that $\sigma_{\min}(\mathbf{A}_{p-1}) \sim m^{0.55}$ and $\sigma_{\min}(\mathbf{A}_1) \sim m^{0.48}$. Fig.20 shows the condition number of



(a) Condition number vs. m ($k=p-1$) (b) Condition number vs. m ($k=1$)



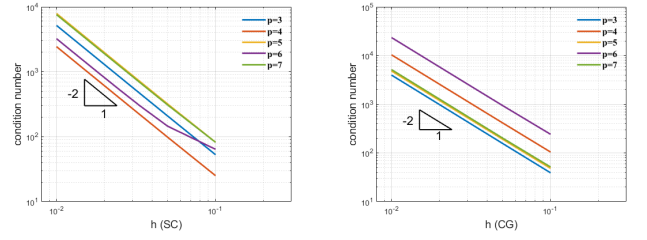
(c) Maximum singular value vs. m ($k=p-1$) (d) Maximum singular value vs. m ($k=1$)



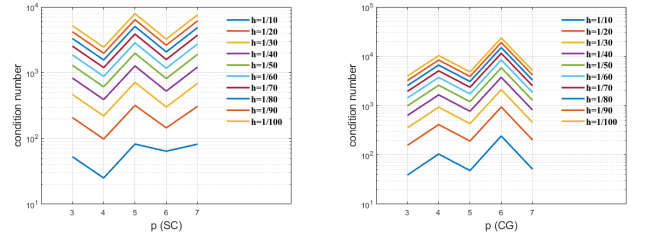
(e) Minimum singular value vs. m ($k=p-1$) (f) Minimum singular value vs. m ($k=1$)

Fig. 19. The maximum/minimum singular value and the spectral condition number of the collocation matrix for different number of collocation points.

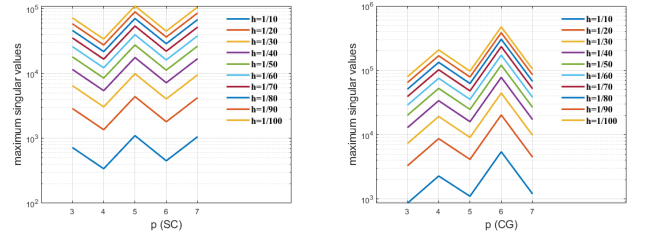
the collocation matrix formed by SC points and CG points versus h and p . From Figs.20(a) and 20(b) we observe that the relationship between the condition number and the mesh size h is similar to the previous results obtained using Greville points. Figs.20(c) and 20(d) show the fluctuation of the condition numbers related to both SC points and CG points for p -refinement. The condition numbers of the collocation matrix formed by SC points in odd-degree cases are lower than those in even-degree cases. On the contrary, for CG points, the spectral properties in even-degree cases are superior to those in odd-degree cases. As shown in Figs.20(e) and 20(f), we find that the variations in condition numbers corresponding to different distributions of collocation points are primarily influenced by the maximum singular values. From Figs.1 and 21, we observe that the SC points in odd-degree cases are more densely distributed near the boundary than those in even-degree cases. Similarly, the CG points show a denser distribution near the boundary for even-degrees than for odd-degrees. The dense distribution of the collocation points increases the L_2 norm of the column vectors corresponding to the basis functions near the boundary, resulting in an uneven distribution of the column vectors. Consequently, the maximum singular value and the condition number increase. A similar explanation can account for the fluctuation of the condition number for CG points with different degrees.



(a) Condition number vs. h (SC) (b) Condition number vs. h (CG)



(c) Condition number vs. p (SC) (d) Condition number vs. p (CG)



(e) Maximum singular value vs. h (SC) (f) Maximum singular value vs. h (CG)

Fig. 20. The spectral condition number and maximum singular value of the collocation matrix formed by SC points and CG points.

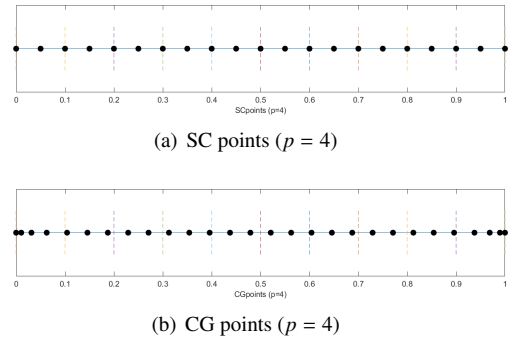


Fig. 21. Distribution of SC points (top) and CG points (bottom) when $p = 4$.

5. Conclusion

In this paper, we conduct a systematic analysis of the spectral properties of the collocation matrix and mass matrix in IGA-L arising from Poisson problem with homogeneous Dirichlet boundary conditions. We focus on the relationship between the condition number, maximum and minimum singular value and the IGA-L discretization parameters h , p , k and the number and distribution of the collocation points. Through numerical investigation, we present theoretical estimations of the condition number, maximum, and minimum singular value of the collocation matrix and mass matrix, filling a gap in the theoretical research in this area. The condition number of the IGA-L collocation ma-

trix for $k = p - 1$ regularity exhibits different behavior in different regions of the (p, h) plane. For small h , the condition number behaves as $h^{-2}p^2$, while for large h , it becomes independent of h and grows exponentially with p . However, the growth rate is slower than that of the stiffness matrix in IGA-G under the same conditions. Therefore, the linear system in IGA-L is better conditioned compared to IGA-G, especially as p increases. For the mass matrix, its condition number is independent of h and grows exponentially with p , with a faster growth rate for $k = 1$ than for $k = p - 1$.

Additionally, we observe that for IGA-L with $k = 1$ regularity, using slightly more collocation points than the number of *dof* can lead to a better-conditioned linear system. Furthermore, the collocation matrix for $k = 1$ contains significantly fewer non-zero entries than for $k = p - 1$, reducing the computational cost of assembling the matrix and solving the linear system.

Future work will focus on enhancing the spectral properties of the collocation matrix by optimizing the distribution and number of collocation points, as well as determining appropriate ranges for mesh size h and degree p . Additionally, we will also consider the extension of this work to advection-diffusion-reaction problems.

References

- [1] T. J. R. Hughes, J. A. Cottrell, Y. Bazilevs, Isogeometric analysis: Cad, finite elements, nurbs, exact geometry and mesh refinement, *Computer Methods in Applied Mechanics and Engineering* 194 (39-41) (2005) 4135–4195. doi:10.1016/j.cma.2004.10.008.
- [2] Y. Bazilevs, L. Beirão da Veiga, J. A. Cottrell, T. J. Hughes, G. Sangalli, Isogeometric analysis: approximation, stability and error estimates for h-refined meshes, *Mathematical Models and Methods in Applied Sciences* 16 (07) (2006) 1031–1090.
- [3] J. A. Cottrell, T. J. Hughes, Y. Bazilevs, *Isogeometric analysis: toward integration of CAD and FEA*, John Wiley & Sons, 2009.
- [4] L. B. Da Veiga, A. Buffa, G. Sangalli, R. Vázquez, Mathematical analysis of variational isogeometric methods, *Acta Numerica* 23 (2014) 157–287.
- [5] T. J. Hughes, A. Reali, G. Sangalli, Duality and unified analysis of discrete approximations in structural dynamics and wave propagation: comparison of p-method finite elements with k-method nurbs, *Computer methods in applied mechanics and engineering* 197 (49-50) (2008) 4104–4124.
- [6] F. Auricchio, L. B. Da Veiga, T. J. R. Hughes, A. Reali, G. Sangalli, Isogeometric collocation methods, *Mathematical Models and Methods in Applied Sciences* 20 (11) (2011) 2075–2107. doi:10.1142/s0218202510004878.
- [7] F. Auricchio, L. B. Da Veiga, T. J. Hughes, A. Reali, G. Sangalli, Isogeometric collocation for elastostatics and explicit dynamics, *Computer methods in applied mechanics and engineering* 249 (2012) 2–14.
- [8] C. Manni, A. Reali, H. Speleers, Isogeometric collocation methods with generalized b-splines, *Computers & Mathematics with Applications* 70 (7) (2015) 1659–1675.
- [9] C. Anitescu, Y. Jia, Y. J. Zhang, T. Rabczuk, An isogeometric collocation method using superconvergent points, *Computer Methods in Applied Mechanics and Engineering* 284 (2015) 1073–1097. doi:10.1016/j.cma.2014.11.038.
- [10] H. Lin, Y. Xiong, X. Wang, Q. Hu, J. Ren, Isogeometric least-squares collocation method with consistency and convergence analysis, *JOURNAL OF SYSTEMS SCIENCE & COMPLEXITY* 33 (5) (2020) 1656–1693. doi:10.1007/s11424-020-9052-9.
- [11] S. DEMKO, On the existence of interpolating projections onto spline spaces, *Journal OF Approximation Theory* 43 (2) (1985) 151–156. doi:10.1016/0021-9045(85)90123-6.
- [12] H. Gomez, L. De Lorenzis, The variational collocation method, *Computer Methods in Applied Mechanics and Engineering* 309 (2016) 152–181. doi:10.1016/j.cma.2016.06.003.
- [13] C. Manni, F. Pelosi, M. L. Sampoli, Generalized b-splines as a tool in isogeometric analysis, *Computer Methods in Applied Mechanics and Engineering* 200 (5-8) (2011) 867–881.
- [14] Y. Bazilevs, V. M. Calo, J. A. Cottrell, J. A. Evans, T. J. R. Hughes, S. Lipton, M. A. Scott, T. W. Sederberg, Isogeometric analysis using t-splines, *Computer methods in applied mechanics and engineering* 199 (5-8) (2010) 229–263.
- [15] K.-J. Bathe, *Finite element procedures*, Klaus-Jurgen Bathe, 2006.
- [16] K. Gahalaut, S. Tomar, Condition number estimates for matrices arising in the isogeometric discretizations, *Johann Radon Institut (RICAM)*, 2012.
- [17] C. Garoni, C. Manni, F. Pelosi, S. Serra-Capizzano, H. Speleers, On the spectrum of stiffness matrices arising from isogeometric analysis, *Numerische Mathematik* 127 (2014) 751–799.
- [18] S. Eisenräger, E. Atroshchenko, R. Makvandi, On the condition number of high order finite element methods: Influence of p-refinement and mesh distortion, *Computers & Mathematics with Applications* 80 (11) (2020) 2289–2339.
- [19] B. Szabó, I. Babuška, *Finite element analysis: Method, verification and validation*.
- [20] C. Canuto, M. Y. Hussaini, A. Quarteroni, T. A. Zang, *Spectral methods: evolution to complex geometries and applications to fluid dynamics*, Springer Science & Business Media, 2007.
- [21] P. Solin, K. Segeth, I. Dolezel, *Higher-order finite element methods*, Chapman and Hall/CRC, 2003.
- [22] L. Demkowicz, *Computing with hp-adaptive finite elements: volume 1 one and two dimensional elliptic and Maxwell problems*, Chapman and Hall/CRC, 2006.
- [23] J. M. Melenk, On condition numbers in hp-fem with gauss-lobatto-based shape functions, *Journal of Computational and Applied Mathematics* 139 (1) (2002) 21–48.
- [24] P. Gervasio, L. Dedè, O. Chanon, A. Quarteroni, A computational comparison between isogeometric analysis and spectral element methods: accuracy and spectral properties, *Journal of Scientific Computing* 83 (2020) 1–45.
- [25] E. Zampieri, L. F. Pavarino, Conditioning and spectral properties of isogeometric collocation matrices for acoustic wave problems, *Advances in Computational Mathematics* 50 (2) (2024) 16.
- [26] L. Piegl, W. Tiller, *The NURBS book*, Springer Science & Business Media, 2012.